A Journal of the Gesellschaft Deutscher Chemiker

Angewandte International Edition GDCh Chemie

www.angewandte.org

Accepted Article

Title: Self-assembled peptide nano-superstructure towards enzyme mimicking hydrolysis

Authors: Ehud Gazit, Yu Chen, Yuqin Yang, Asuka A. Orr, Pandeeswar Makam, Boris Redko, Elvira Haimov, Yannan Wang, Linda J. W. Shimon, Sigal Rencus-Lazar, Meiting Ju, Phanourios Tamamis, and Hao Dong

To be cited as: *Angew. Chem. Int. Ed.* 10.1002/anie.202105830

Link to VoR: https://doi.org/10.1002/anie.202105830

WILEY-VCH

10.1002/anie.202105830

RESEARCH ARTICLE

WILEY-VCH

Self-assembled peptide nano-superstructure towards enzyme mimicking hydrolysis

Yu Chen† [a], Yuqin Yang† [b], Asuka A. Orr† [c], Pandeeswar Makam[d], Boris Redko[e], Elvira Haimov[e], Yannan Wang[f], Linda J. W. Shimon[g], Sigal Rencus-Lazar[a], Meiting Ju[f], Phanourios Tamamis*[c], Hao Dong*[b], Ehud Gazit*[a][h]

[a] Dr. Y. Chen, Dr. S. Rencus-Lazar, Prof. E. Gazit
The Shmunis School of Biomedicine and Cancer Research, Tel Aviv University, Israel
E-mail: ehudga@tauex.tau.ac.il
[b] Y. Yang, Prof. Hao Dong
Kuang Yaming Honors School & Institute for Brain Sciences, Nanjing University, China
E-mail: donghao@nju.edu.cn
[c] A. A. Orr, Prof. P. Tamamis
Artie McFerrin Department of Chemical Engineering, Texas A&M University, College Station, Texas, United States
E-mail: tamamis@tamu.edu
[d] Dr. P. Makam
Department Applied Chemistry, IIT(BHU), Varanasi, India
[e] Dr. B. Redko, Dr. E. Haimov
BLAVATNIK CENTER for Drug Discovery, Tel Aviv University, Israel
[f] Y. Wang, Prof. M. Ju
National & Local Joint Engineering Research Center on Biomass Resource Utilization, Nankai University, China
[g] Dr. L. J. W. Shimon
Department of Chemical Research Support, Weizmann Institute of Science, Rehovot, Israel
[h] Prof. E. Gazit
Department of Materials Science and Engineering, Tel Aviv University, Israel

Supporting information for this article is given via a link at the end of the document.

Abstract: The structural arrangement of amino acid residues in native enzymes underlies their remarkable catalytic properties, thus providing a notable point of reference for designing potent yet simple biomimetic catalysts. Herein, we describe a minimalistic approach to construct a dipeptide-based nano-superstructure with enzyme-like activity. The self-assembled biocatalyst comprises one peptide as a single building block, readily synthesized from histidine. Through coordination with zinc ion, the peptide self-assembly procedure allows the formation of supramolecular β-sheet ordered nanocrystals, which can be used as basic units to further construct higher-order superstructure. As a result, remarkable hydrolysis activity and enduring stability are demonstrated. Our work exemplifies the use of a bioinspired supramolecular assembly approach to develop next-generation biocatalysts for biotechnological applications.

Introduction

A considerable number of enzymes with fascinating activity have naturally evolved to control complex chemical processes with extraordinary efficiency and selectivity[1]. As one of the most ubiquitous metalloenzymes, carbonic anhydrases (CA) are found in most organisms in all kingdoms of life and are involved in diverse physiological functions, including respiration and cellular pH maintenance[2]. Specifically, as an effective hydrolase, CAII is of great significance in industrial "small molecule" chemical conversion. With the insights obtained from the X-ray crystallographic structure of CAII, significant progress has been successfully made in the *de novo* design of protein scaffolds to catalyze biological reactions[3]. In addition to the evolution of these large molecules based artificial enzymes, the "bottom-up" approach for the fabrication of complex nanomaterials has also spawned new developments in this direction and provided scientists with an ever-evolving toolbox of artificial enzymes[4]. Enzyme-inspired supramolecular catalysts hold great promise in medical and industrial biotransformation applications[5]. In particular, peptides and peptide derivatives are predominantly attractive components for constructing supramolecular catalysts, as evidenced by the fact that complex enzymes in biological systems comprise mainly of the 20 genetically-encoded amino acids. The development of such an enzyme-inspired peptide supramolecular catalyst is expected to offer a more robust and efficacious alternative to industrial and academic enzymatic catalysis and more in-depth insight into the origin of the native enzyme[6].

Guided by the minimalistic principle originally described by DeGrado[7], various catalytic self-assembling peptide structural units derived from amyloid sequences have been discovered[6a, 8]. Korendovych and coworkers designed a series of amyloid-like fibril heptapeptide-based supramolecular esterase with alternating hydrophobic and hydrophilic residues[9]. The resulting peptide library was screened for catalyzing the hydrolysis of acyl esters in the presence of zinc. Although catalytic peptide assemblies discovered in these pioneering studies are very promising, several intrinsic drawbacks, including high costs of preparation and purification, low operational stability, and inefficient recycling and reuse, severely hamper their widespread applications[8a, 10].

Cyclic dipeptides, as the smallest cyclic peptides, have complex side-chain substituents, which can be used as a model to mimic a catalytic active site[11]. The versatile hydrogen bonding capabilities of the diketopiperazine motif form a unique and stable packing arrangement, which can be used as a robust scaffold to overcome the problem of enzymatic degradation[12]. Here, inspired by the structure of the active site of CAII, we aimed to incorporate histidine residues into one short peptide segment, which will serve as the basic building block of a supramolecular catalyst. For this purpose, we used cyclic-dihistidine (cyclo-HH) as a building block to prepare a supramolecular assembly-based nano-superstructure with hydrolytic activity through a simple and general method (**Scheme 1**). The self-assembly mechanism of cyclo-HH and zinc iodide (cyclo-HH-ZnI_2) was investigated using all-atom molecular dynamics (MD) simulations and X-ray crystallography analysis. The cyclo-HH-ZnI_2 nanowires displayed hydrolytic activity, with exceptional stability and recyclability. The activity of the catalyst was retained after five cycles, making it more robust and durable than other biomolecular artificial hydrolase complexes. Moreover, using hydrolytic catalysis as a model reaction, theoretical calculations and experimental studies unambiguously identified that the rate-determining step of the entire reaction was the nucleophilic attack process, and the confined local environment was critical for hydrolysis.

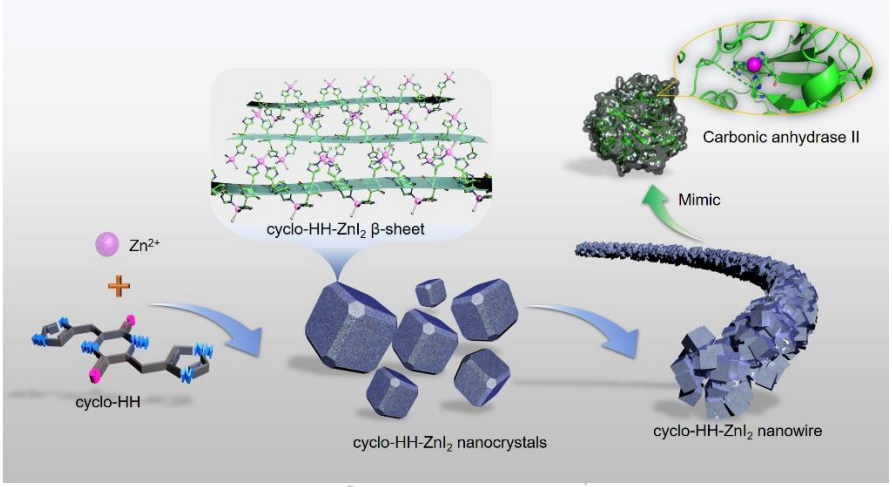

Scheme 1. Design of a cyclic dipeptide supramolecular assembly-based nano-superstructure for mimicking the molecular structure of the active site of CAII.

Results and Discussion

Cyclic dipeptides represent a large class of secondary metabolites containing 2,5-diketopiperazine heterocycles, which are ubiquitous and evolutionarily conserved in various organisms[13]. They were also identified as chemical degradation products in roasted coffee, which contributes to the perceived bitterness. Inspired by this thermal treatment process, cyclo-HH was first synthesized using an eco-friendly microwave-assisted solid-phase peptide method[14] (**Figure 1a, Figure S1-S3**). To allow self-assembly, cyclo-HH was mixed with ZnI_2 under controlled hydrothermal conditions, resulting in nanostructure formation. The one-dimensional nanowire morphology of the resulting cyclo-HH-ZnI_2 assemblies was observed by scanning electron microscopy (SEM) and transmission electron microscopy (TEM) (**Figure 1b-d**). Interestingly, the large-scale, well-dispersed nanoparticles with an average size of 10 nm could be detected in high-resolution images, indicating that the nanowire superstructures were indeed composed of numerous nanoparticles. The powder X-ray diffraction (PXRD) pattern (**Figure 1e**) of the cyclo-HH-ZnI_2 nanowires exhibited high crystallinity.

Furthermore, we performed fluorescence excitation-emission matrix contour profile and confocal fluorescence lifetime microscopy (FLIM) studies of the photodynamic properties of the cyclo-HH-ZnI_2 nanowires[15]. Upon excitation at 400 nm, the cyclo-HH-ZnI_2 nanowires exhibited bright fluorescence emission centered at 500 nm (**Figure S4**). The lifetime image and phasor approach analysis revealed the high homogeneity of the cyclo-HH-ZnI_2 nanowire superstructure with a uniform fluorescence lifetime of approximately 2.3 ns[16] ((**Figure 1f**, **Figure S5-S7**). The porosity of the cyclo-HH-ZnI_2 nanowire superstructure was investigated by measuring the N_2 adsorption at 77 K. The Brunner-Emmet-Teller (BET) surface area and pore volume were calculated to be as high as 257.36 m^2/g and 0.45 cm^3/g, respectively. An extensive N_2 uptake below 0.1 P/P_0 indicating extensive microporosity and a distinct capillary condensation step at higher relative pressures (P/P_0 = 0.7 to 1) were also recorded, demonstrating the formation of mesoporosity (**Figure 1g, Figure S8**). The observed mesopores were attributed to the void space between cyclo-HH-ZnI_2 nanocrystals, enforced by their hierarchical arrangement in the microstructure, as observed in **Figure 1d**. These cyclo-HH-ZnI_2 multiporous structures may host abundant catalytic active sites and provide flexible transport pathways to diffuse reactants during the hydrolytic process, and therefore could be extremely useful in hydrolysis[10h, 17].

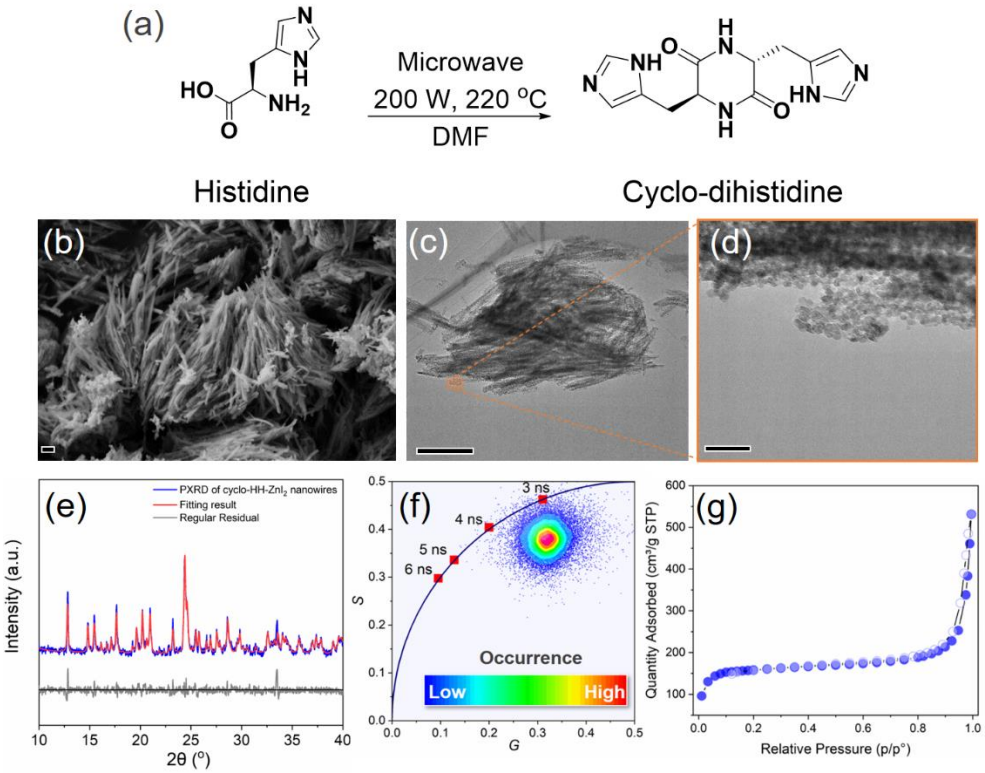

Figure 1. Characterization of the cyclo-HH-ZnI_2 nanowires. (a) One-step synthesis of cyclo-HH via a simple microwave-assisted solid-phase peptide method. (b) SEM and (c, d) TEM images of as-synthesized cyclo-HH-ZnI_2 nanowires. The yellow dashed frame in (c) indicates the area selected for high-magnification imaging shown in (d). Scale bars, 200 nm, 500 nm, and 50 nm (b to d, respectively). (e) Fitting of the experimental PXRD of cyclo-HH-ZnI_2 nanowires (blue) and calculated diffractogram of cyclo-HH-ZnI_2 single crystal (red). The grey line represents the difference between the diffractograms. (f) Two-dimensional histogram phasor plots generated from FLIM images of cyclo-HH-ZnI_2 nanowires. The colors correspond to the occurrence frequency. (g) N_2 adsorption isotherms of cyclo-HH-ZnI_2 nanowires (filled circles: adsorption, empty: desorption).

MD simulations can be powerful tools in providing insights into molecular self-assembly by analyzing the initial nucleation of molecules in different environments[18]. Here, we performed multiple multi-ns explicit solvent MD simulations in CHARMM[19] to investigate the initial stages of cyclo-HH self-assembly in the presence of Zn^{2+} and iodide ions. Across all simulations, visual inspection confirmed that highly disordered aggregates of cyclo-HH molecules broke apart and reformed, indicating that the cyclo-HH molecules were not trapped in a local energetic minimum in a given simulation and facilitated higher-order structures. Within the simulations, ordered antiparallel and parallel configurations of cyclo-HH dimers were observed, with the former being the predominant configuration (Figure S9, Table S1), in line with the crystallographic data (Table S2). According to the time-evolution structural analysis of the antiparallel configurations (**Figure S9, Table S1**), the elementary unit formation began from coordinating the two histidine side chains of two cyclo-HH molecules with a Zn^{2+} ion (**Figure 2a i-ii**). Subsequently, two cyclo-HH molecules coordinating with Zn^{2+} began forming hydrogen bond interactions between their backbone atoms to eventually form antiparallel β-bridge configurations. (**Figure 2a iii-iv**). These β-sheet-like dimeric conformations could constitute the elementary units that comprise the self-assembled clusters and subsequently the larger crystals.

To validate our hypothesis and further characterize the specific self-assembly mechanism, we extended the solvothermal reaction time to crystalize the micrometer-sized cyclo-HH-ZnI_2 single crystals (**Figure S10, S11**) and analyzed the resulting structures *via* X-ray crystallography (**Table S2**). The simulated diffractogram from the single-crystal was vastly consistent with the pattern of the cyclo-HH-ZnI_2 nanowire, indicating a similar molecular organization (**Figure 1e, S12**). Cyclo-HH-ZnI_2 crystallized in the orthorhombic space group Pbcn, with one cyclo-HH molecule, one neutral $[Zn(L)_2I_2]$ unit per asymmetric unit (**Figure 2b**). The Zn(II) ion was attached with two iodine ligands and further coordinated with two nitrogen atoms from the imidazole groups on two different cyclo-HH molecules, providing a central coordination site geometric tetrahedron (**Figure 2c**). The diketopiperazine rings on two adjacent cyclic dipeptides were linked through β-sheets hydrogen bonding with N — H···O = C

(donor···acceptor) distances of 2.86 Å and 2.83 Å (**Figure 2d**). It is worth noting that the antiparallel configurations of cyclo-HH dimers observed within the simulations (Figure 2a iv) were in line with the X-ray crystal structure (Figure 2b-d). Upon structural alignment of all the antiparallel dimer configurations derived from the simulations to the X-ray crystal structure, the root-mean-square deviation of the cyclo-HH dimer heavy atoms was found to be only 1.93 ± 0.66 Å. Interestingly, the *cis*- and *trans*-conformational cyclic dipeptides bridged zinc ions to form unusual *meso*-helix motifs in one single strand along the *b*-axis, giving rise to an infinite one-dimensional chain (**Figure S13**). Furthermore, these discrete *meso*-helical chains were interconnected by π-π stacking interactions of imidazole rings (**Figure S14**), thereby further stabilizing the crystal structure (**Figure 2e**).

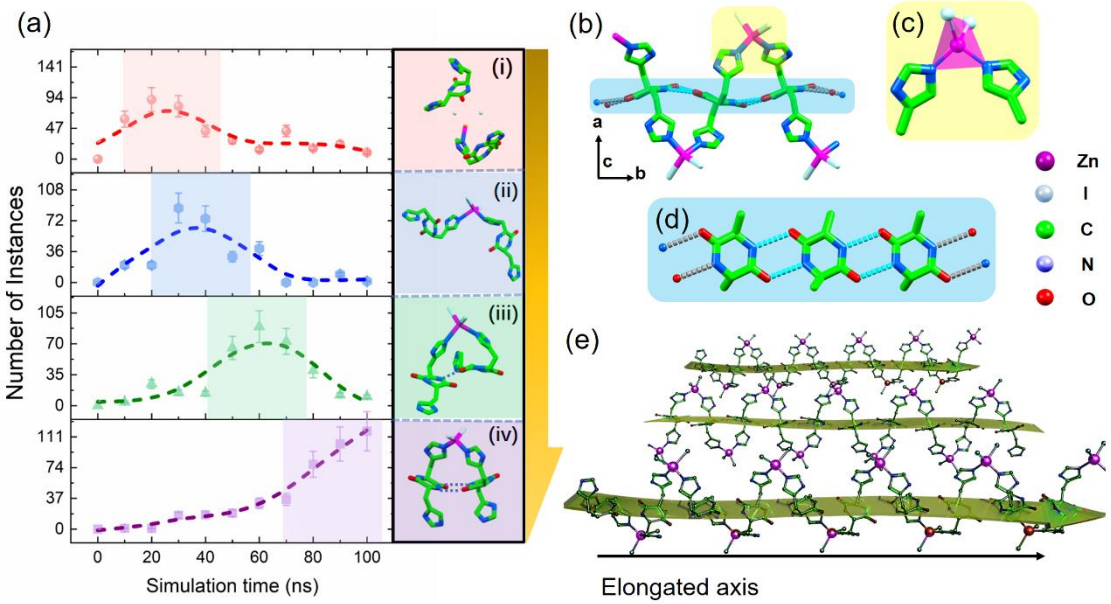

Figure 2. Structural analysis of the cyclo-HH-ZnI_2 assemblies. (a) The number of instances of interactions for molecules eventually forming antiparallel configurations within the simulations. The tracked interactions are: (i) one imidazole ring of a cyclo-HH molecule coordinating with one ZnI_2 (red), (ii) two imidazole rings belonging to opposing cyclo-HH molecules coordinating with a single ZnI_2 (blue), (iii) two cyclo-HH molecules forming one hydrogen bond between their backbones while coordinating with a single ZnI_2 (green), and (iv) two cyclo-HH molecules forming an antiparallel configuration while coordinated with ZnI_2 (purple). Representative illustration of the cyclo-HH and ZnI_2 self-assembly process into a β-sheet-like elementary structure, as detected by MD simulations and structural analysis software, is shown. (b) Single-crystal structure of cyclo-HH-ZnI_2 in Pbcn space group. Color code: green, C; red, O; blue, N; purple, Zn; and cyan, Iodine. (c) Zn(II)-centered geometric tetrahedron: a Zn(II) atom coordinated with two ligands and two N-donor atoms from the imidazole groups of two different cyclo-HH molecules. (d) β-sheets hydrogen bonding connecting two adjacent cyclic-dipeptides. (e) 3D supramolecular structure packed between the imidazole rings of adjacent 1D chains.

Next, we sought to examine the hydrolytic activity of the cyclo-HH-ZnI_2 nanowires [20]. For this purpose, *p*-nitrophenyl acetate (pNPA) hydrolysis was used as a probe reaction (**Figure 3a**). **Figure 3b** shows the most energetically favored binding mode of the pNPA substrate according to molecular docking using AutoDock4$_{Zn}$[21] (with an affinity of -5.8 kcal mol^{-1} based on the AutoDock4$_{Zn}$[21] scoring function). Owing to the confined spatial environment formed between the discrete meso-helical chains, it appears that the pNPA substrate molecules can be aligned between cyclo-HH-ZnI_2 β-sheet-like grooves (**Figure S15**), where each substrate is sufficiently proximal for nucleophile attacks. In the most energetically favored binding mode, pNPA was stabilized through a hydrogen bond between its ester carbonyl group and a cyclo-HH imidazole ring NH group, as well as a hydrogen bond between its nitro group and a separate cyclo-HH imidazole ring NH group (**Figure 3b**). Additionally, the ester group was in close proximity to the bound Zn^{2+} ion (**Figure 3b**). Overall, as the hydrolysis of pNPA occurs at the ester group, the resulting structures could be indicative of cyclo-HH-ZnI_2 potential biocatalytic activity.

The hydrolysis activity of cyclo-HH-ZnI_2 nanowires towards pNPA was investigated by monitoring the time-dependent absorbance changes of the reaction product, *p*-nitrophenol (pNP), at 405 nm. Interestingly, cyclo-HH-ZnI_2 nanowires were found to be capable of ester hydrolysis, as in the presence of the cyclo-HH-ZnI_2 nanowire catalyst, the colorless pNPA solution turned yellow, indicating the formation of the reaction product pNP. Moreover, increasing concentrations of cyclo-HH-ZnI_2 nanowires resulted in an evident enhancement of the reaction rate (**Figure 3c, Figure S16**). In

contrast, under similar conditions, the control substrate solution without the catalyst did not show any visible color change. The enzymatic kinetics of the cyclo-HH-ZnI_2 nanowires was further studied to characterize the enzyme-like properties. By changing the concentration of the pNPA substrate while keeping the catalyst concentration constant (**Figure 3d**), the reactant adsorption equilibrium constant (K_α) could be calculated as 0.232 mM, with a maximum initial velocity (V_{max}) of 1.32×10^{-3} mM s^{-1}. Notably, the calculated catalytic efficiency[22] (k_{cat}/K_α, where k_{cat} is the turnover number) was 93.21 M^{-1} s^{-1}. With the same absolute molarity (0.063 mM), the peptide building block cyclo-HH showed an approximately 6-fold reduced activity compared to cyclo-HH-ZnI_2 nanowire, revealing the fact that the differences in the microenvironment at the active sites of the Zn(II) coordination tetrahedron may account for the major difference in catalytic activity[5b, 10d, 10f] (**Figure S17**). Furthermore, a control experiment using cyclo-HH-ZnI_2 single crystal as a catalyst showed that its activity was approximately 3-fold lower than that of cyclo-HH-ZnI_2 nanowires (**Figure 3d**), indicating the catalytic rate is greatly affected by the size of the biocatalyst, which was attributed to the increased catalytic surface area with abundant catalytic active sites[10h, 23]. To assess the substrate specificity, cyclo-HH-ZnI_2 nanowires were mixed with various nitrophenyl esters comprising different side-chain lengths, and the catalytic activity was assayed (**Figure S18**). Cyclo-HH-ZnI_2 nanowires showed excellent catalytic activity towards two other ester substrates, namely 4-nitrophenyl butyrate (pNPB) and 4-nitrophenyl valerate (pNPV). The catalytic stability of the cyclo-HH-ZnI_2 nanowire catalyst was also assessed. As shown in **Figure S19**, when the ZnI_2 nanowires were stored in the air at room temperature for 30 days, the original catalytic activity was still retained, and no significant decrease in the activity was observed. Moreover, the cyclo-HH-ZnI_2 nanowires could be easily separated from the product compound for recycling purposes, and retaining more than 80% of the initial activity even after five cycles of use (**Figure 3e**). The decreased activity may be due to the redispersion and agglomeration of the nanoparticles during washing and centrifuging (**Figure S20**).

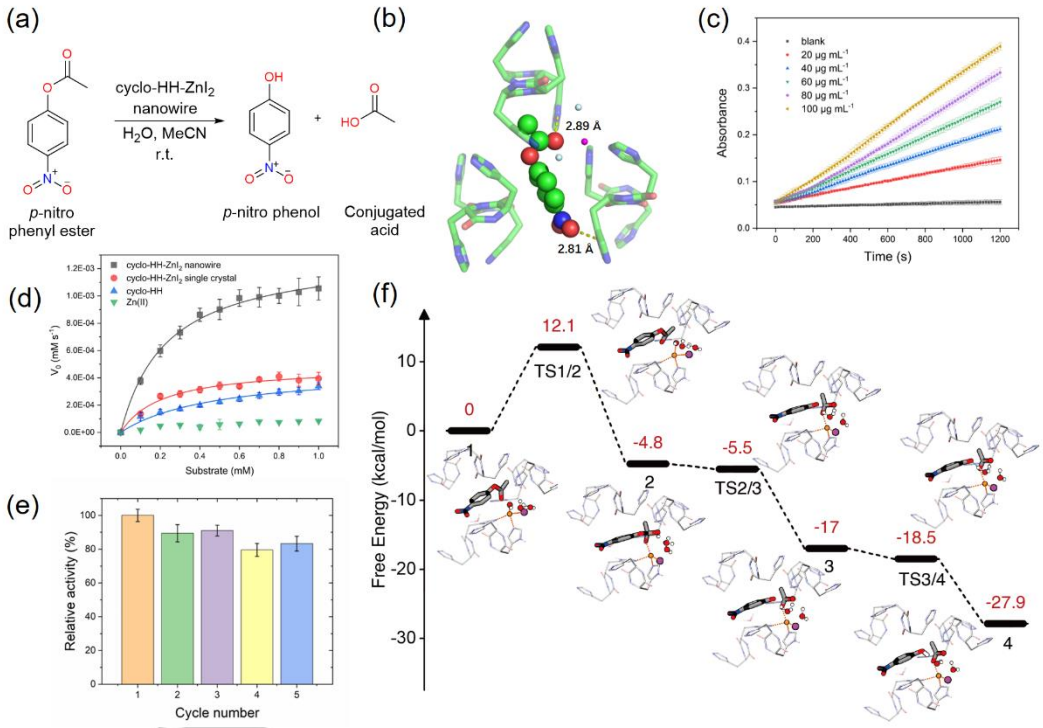

Figure 3. The ester hydrolysis activity of cyclo-HH-ZnI_2 nanowires. (a) Schematic illustration of ester hydrolysis catalyzed by cyclo-HH-ZnI_2 nanowires. (b) Docked structure of *p*-nitrophenyl acetate (pNPA) bound to the cyclo-HH-ZnI_2 slab based on the crystal structure. (c) Time-dependent absorbance at 405 nm during pNPA hydrolysis in the presence of different doses of cyclo-HH-ZnI_2 nanowires. The blank sample represents a buffer-only control (PBS, pH=7.4). (d) Steady-state kinetic assay of pNPA hydrolysis reaction in the presence of cyclo-HH-ZnI_2 nanowires, cyclo-HH-ZnI_2 single crystal, and cyclo-HH and Zn(II). (e) Relative activity of cyclo-HH-ZnI_2 nanowires in pNPA hydrolysis reaction during recycling and reuse. (f) Catalytic reaction mechanism and the optimized structures along the reaction pathway. A cluster containing key groups around the catalytic center is shown. Only the hydrogen atoms bonded to nitrogen or oxygen in the catalytic center are shown for clarity. The zinc and iodide atoms are represented as gray and pink balls, respectively.

Following the experimental characterization of the catalytic esterase activity of the cyclo-HH-ZnI_2 nanowires, we carried out first-principle density functional theory calculations to study the catalytic reaction path starting from a possible binding mode of pNPA to cyclo-HH-ZnI_2, as shown in **Figure 3f**. Particularly in this structure, the ester group of pNPA was located near the active site, defined as a coordinated Zn^{2+} ion with the neighboring groups: the Zn^{2+} ion was bound to two imidazole rings of histidine residues and coordinated by two iodine ions, as revealed by the X-ray structure. Then, one iodine ion of the active site was replaced by a hydroxyl group, which was expected to exert a nucleophilic attack of the ester bond in the following reaction path, as we previously shown in a relevant system[10e]. We added three water molecules around the hydroxyl group in the model to stabilize the system. The chemical environment around the active site was also reserved to mimic the restricted environment of the reaction. The initial structure of complex**1** was based on the docking structure representing a possible binding mode of pNPA towards the cyclo-HH-ZnI_2 cluster. The reaction took place in the chemically confined environment, and the steric hindrance restricted the orientation of the substrate during the reaction pathway. The subsequent bond formation between the carbon atom of the carbonyl group of pNPA and the oxygen atom of the hydroxide ion (bound to the Zn atom) led to an intermediate complex**2**. This nucleophilic attack of the hydroxyl ligand occurred through the transition state (**TS1/2**), where the carbonyl group's carbon atom was close to the hydroxide ion's oxygen atom. Importantly, this was calculated to be the rate-determining step along the reaction path, with a Gibbs free energy barrier $\Delta G^{\neq}$ = 12.1 kcal/mol. Consequently, the C1-O5 bond cleaved through **TS2/3** to convert the hydrolysis products, an acetic acid moiety and a *p*-nitrophenoxide anion, as shown in complex**3**. The conversion of complex **2** to **3** is exceedingly exothermic, with ΔG^0 = -12.2 kcal/mol. Finally, one proton transferred from the acetic acid moiety to the *p*-nitrophenoxide anion through a water molecule, as shown in **TS3/4,** leading to the single hydrolysis product (pNP) (in complex **4**). Furthermore, the proton transferred from the distal imidazole moiety to the acetoxyl group, where the other acetic acid product was formed, and the original complex was restored[10e]. The release of the acetic acid molecule from the active site and the subsequent binding of a new water molecule to the active site re-initiated the entire process.

Conclusion

In summary, inspired by the structure of the active site of CAII, we successfully constructed a simple cyclo-dipeptidyl supramolecular nano-superstructure and implemented an effective hydrolysis biocatalyst according to the concept of minimalistic *de novo* design. Unlike natural enzymes composed of hundreds of amino acid sequences, the newly-designed cyclo-HH-ZnI_2 biocatalyst utilizes only a cyclo-dipeptide as the single building block, and can be easily synthesized using the environmentally friendly microwave-assisted solid-phase peptide method. Through coordination with zinc ions, the cyclo-HH self-assembly process can be well controlled to produce zero-dimensional, homogeneous nanostructures, which can then be used as basic units to form a higher-order nanoarchitecture. The superstructure nano-assembly contains abundant catalytic active sites and can provide a flexible transportation route for the diffusion of reactants in the hydrolysis process. As a result, an effective hydrolytic activity of 93.21 M^{-1} s^{-1} can be achieved.

Additionally, the cyclo-HH-ZnI_2 biocatalyst is strikingly stable under long storage and markedly reusable, which is of great significance in the field of industrial "small molecule" chemical conversion. Moreover, quantum mechanics calculations were used to probe the catalytic effect, indicating that the reaction rate-determining step is the nucleophilic attack process. Moreover, the steric hindrance of the local environment of the cyclo-HH-ZnI_2 biocatalyst restricts the orientation of the substrate during the reaction, which is essential for efficient hydrolysis. This simple supramolecular strategy provides an attractive new alternative to state-of-the-art biocatalysts, and can be further extended to fabricate other artificial biocatalysts toward robust and efficient chemical transformations.

Acknowledgements

Y. Chen, Y.Q. Yang and A.A. Orr, contributed equally to this work. This work was supported in part by the European Research Council under the European Union Horizon 2020 research and innovation program (No. 694426) (E.G.), Joint NSFC-ISF Grant (no. 3145/19) (E.G.), National Natural Science Foundation of China (No. 21833002) (H.D.), and Natural Science Foundation of Jiangsu Province (No. BK20190056) (H.D.). Y. Chen acknowledges the Center for Nanoscience and Nanotechnology at Tel Aviv University for financial support. A.A. Orr acknowledges Texas A&M University Graduate Diversity Fellowship from the TAMU Office of Graduate and Professional Studies. MD simulations and associated calculations were conducted using the Ada supercomputing cluster at the Texas A&M High Performance Research Computing Facility, and additional computational resources available to P.T. at Texas A&M University. Parts of the calculations were performed using computational resources on an IBM Blade cluster system from the High-Performance Computing Center (HPCC) of Nanjing University. The authors thank Mariana Hildebrand, Leeor Kronik and the members of the Dong, Tamamis and Gazit laboratories for helpful discussions.

Competing Interests

The authors declare no competing interests.

Keywords: biocatalysis • peptide • self-assembly • nano-superstructure • supramolecular chemistry

[1] aF. H. Arnold, *Nature* **2001**, *409*, 253-257; bM. Frenkel-Pinter, M. Samanta, G. Ashkenasy, et al., *Chemical Reviews* **2020**, *120*, 4707-4765.
[2] C. M. Maupin, N. Castillo, S. Taraphder, et al., *J. Am. Chem. Soc.* **2011**, *133*, 6223-6234.
[3] aS. Toba, G. Colombo, K. M. Merz, *J. Am. Chem. Soc.* **1999**, *121*, 2290-2302; bM. L. Zastrow, A. F. A. Peacock, J. A. Stuckey, et al., *Nature Chemistry* **2012**, *4*, 118-123; cW. J. Song, F. A. Tezcan, *Science* **2014**, *346*, 1525.
[4] aC. Wang, J. Fei, K. Wang, et al., *Angewandte Chemie International Edition* **2020**, *59*, 18960-18963; bL. Huang, J. Chen, L. Gan, et al., *Science Advances* **2019**, *5*, eaav5490; cD. Jiang, D. Ni, Z. T. Rosenkrans, et al., *Chemical Society Reviews* **2019**, *48*, 3683-3704; dM. Liang, X. Yan, *Accounts of Chemical Research* **2019**, *52*, 2190-2200.
[5] aJ. Wang, R. Huang, W. Qi, et al., *Applied Catalysis B: Environmental* **2019**, *254*, 452-462; bM. D. Nothling, A. Ganesan, K. Condic-Jurkic, et al., *Chem* **2017**, *2*, 732-745; cJ. Chen, L. Huang, Q. Wang, et al., *Nanoscale* **2019**, *11*, 5960-5966; dW.-H. Chen, M. Vázquez-González, A. Zoabi, et al., *Nature Catalysis* **2018**, *1*, 689-695; eA. P. Katsoulidis, K. S. Park, D. Antypov, et al., *Angewandte Chemie International Edition* **2014**, *53*, 193-198; fQ. Liu, K. Wan, Y. Shang, et al., *Nature Materials* **2020**.
[6] aK. Tao, P. Makam, R. Aizen, et al., *Science* **2017**, *358*, eaam9756; bS. I. Stupp, L. C. Palmer, *Chemistry of Materials* **2014**, *26*, 507-518; cS. Bolisetty, R. Mezzenga, *Nat. Nanotechnol.* **2016**, *11*, 365-371; dA. Lampel, S. A. McPhee, H.-A. Park, et al., *Science* **2017**, *356*, 1064; eB. Sun, K. Tao, Y. Jia, et al., *Chemical Society Reviews* **2019**, *48*, 4387-4400; fX. Li, J. Fei, Y. Xu, et al., *Angewandte Chemie* **2018**, *130*, 1921-1925.
[7] aR. P. Cheng, S. H. Gellman, W. F. DeGrado, *Chem. Rev.* **2001**, *101*, 3219; bW. F. DeGrado, Z. R. Wasserman, J. D. Lear, *Science* **1989**, *243*, 622.
[8] aL. R. Marshall, O. Zozulia, Z. Lengyel-Zhand, et al., *ACS Catal.* **2019**, *9*, 9265-9275; bT. J. Moyer, J. A. Finbloom, F. Chen, et al., *J. Am. Chem. Soc.* **2014**, *136*, 14746-14752; cA. Levin, T. A. Hakala, L. Schnaider, et al., *Nature Reviews Chemistry* **2020**, *4*, 615-634; dT. P. J. Knowles, M. J. Buehler, *Nat. Nanotechnol.* **2011**, *6*, 469-479.
[9] C. M. Rufo, Y. S. Moroz, O. V. Moroz, et al., *Nature Chemistry* **2014**, *6*, 303-309.
[10] aC. Zhang, X. Xue, Q. Luo, et al., *ACS Nano* **2014**, *8*, 11715; bM. D. Nothling, Z. Xiao, A. Bhaskaran, et al., *ACS Catal.* **2019**, *9*, 168-187; cO. Zozulia, M. A. Dolan, I. V. Korendovych, *Chem. Soc. Rev.* **2018**, *47*, 3621; dA. M. Garcia, M. Kurbasic, S. Kralj, et al., *Chemical Communications* **2017**, *53*, 8110-8113; eR. Song, X. Wu, B. Xue, et al., *J. Am. Chem. Soc.* **2019**, *141*, 223-231; fA. J. Kleinsmann, B. J. Nachtsheim, *Organic & Biomolecular Chemistry* **2020**, *18*, 102-107; gT. O. Omosun, M.-C. Hsieh, W. S. Childers, et al., *Nature Chemistry* **2017**, *9*, 805-809; hP. Makam, S. S. R. K. C. Yamijala, K. Tao, et al., *Nature Catalysis* **2019**; iA. Lampel, R. V. Ulijn, T. Tuttle, *Chemical Society Reviews* **2018**, *47*, 3737-3758; jM. Lee, T. Wang, O. V. Makhlynets, et al., *Proceedings of the National Academy of Sciences* **2017**, *114*, 6191; kO. Zozulia, I. V. Korendovych, *Angewandte Chemie International Edition* **2020**, *59*, 8108-8112; lC. Zhang, R. Shafi, A. Lampel, et al., *Angew. Chem., Int. Ed.* **2017**, *56*, 14511.
[11] aI. Bellezza, M. J. Peirce, A. Minelli, *Trends in Molecular Medicine* **2014**, *20*, 551-558; bR. Zou, Q. Wang, J. Wu, et al., *Chemical Society Reviews* **2015**, *44*, 5200-5219; cA. Mantion, L. Massüger, P. Rabu, et al., *J. Am. Chem. Soc.* **2008**, *130*, 2517-2526.
[12] S. Palacin, D. N. Chin, E. E. Simanek, et al., *J. Am. Chem. Soc.* **1997**, *119*, 11807-11816.
[13] T. W. Giessen, M. A. Marahiel, *Frontiers in Microbiology* **2015**, *6*.
[14] L. Pérez-Picaso, J. Escalante, H. F. Olivo, et al., *Molecules* **2009**, *14*, 2836-2849.
[15] aZ. Fan, L. Sun, Y. Huang, et al., *Nat. Nanotechnol.* **2016**, *11*, 388; bJ. Kong, J. Zhang, Y. Wang, et al., *ACS Applied Materials & Interfaces* **2020**, *12*, 31830-31841.
[16] B. M. Connolly, M. Aragones-Anglada, J. Gandara-Loe, et al., *Nature Communications* **2019**, *10*, 2345.
[17] B. Wang, P. Prinsen, H. Wang, et al., *Chemical Society Reviews* **2017**, *46*, 855-914.
[18] K. Tao, Y. Chen, A. A. Orr, et al., *Advanced Functional Materials* **2020**, *30*, 1909614.
[19] B. R. Brooks, C. L. Brooks Iii, A. D. Mackerell Jr, et al., *Journal of Computational Chemistry* **2009**, *30*, 1545-1614.
[20] M. O. Guler, S. I. Stupp, *J. Am. Chem. Soc.* **2007**, *129*, 12082.
[21] D. Santos-Martins, S. Forli, M. J. Ramos, et al., *Journal of Chemical Information and Modeling* **2014**, *54*, 2371-2379.
[22] B. Jiang, D. Duan, L. Gao, et al., *Nature Protocols* **2018**, *13*, 1506-1520.
[23] F. Yang, D. Deng, X. Pan, et al., *National Science Review* **2015**, *2*, 183-201.

Entry for the Table of Contents

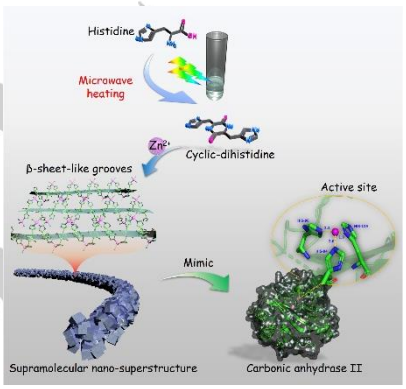

The peptide nano-superstructure employs a cyclic dipeptide as a building block, is inspired by the coffee roasting process, and can be easily synthesized. The self-assembled biocatalyst displays enzyme-like hydrolysis activity, with exceptional stability and recyclability. This catalytic peptide assembly provides a potent complement for minimalistic biocatalysts and offers an attractive alternative to the current arsenal of natural metalloenzymes.